Food Research International 105 (2018) 423–431

Contents lists available at ScienceDirect

Food Research International

journal homepage: www.elsevier.com/locate/foodres

Non-triglyceride components modulate the fat crystal network of palm kernel oil and coconut oil

Xiuhang Chai[a], Zong Meng[a], Jiang Jiang[a], Peirang Cao[a], Xinyu Liang[b], Michael Piatko[c], Shawn Campbell[c], Seong Koon Lo[b,c], Yuanfa Liu[a,*]

[a] State Key Laboratory of Food Science and Technology, Synergetic Innovation Center of Food Safety and Nutrition, School of Food Science and Technology, Jiangnan University, 1800 Lihu Road, Wuxi 214122, Jiangsu, People's Republic of China
[b] Rich Products Corporation, 75 Suhong West Road, Suzhou 21520, Jiangsu, People's Republic of China
[c] Rich Products Corporation, One Robert Rich Way, Buffalo, NY 14213, United States

ARTICLE INFO

Keywords:
Indigenous minor components
Crystallization behavior
Polymorphism
Microstructure
Fat crystal network
Fractal dimension

ABSTRACT

PKO and CNO are composed of 97–98% triacylglycerols and 2–3% minor non-triglyceride components (FFA, DAG and MAG). Triglycerides were separated from minor components by chromatographic method. The lipid composition, thermal properties, polymorphism, isothermal crystallization behavior, nanostructure and microstructure of PKO, PKO-TAG, CNO and CNO-TAG were evaluated. Removal of minor components had no effect on lipid composition and equilibrium solid fat contents. However, presence of minor components did increase the slip melting point and promoted the onset of crystallization from DSC crystallization profiles. The thickness of the nanoscale crystals increased with no polymorphic transformation after removing the minor components. Crystallization kinetics revealed that minor components decreased crystal growth rate with higher $t_{1/2}$. Sharp changes in the values of the Avrami constant k and exponent n were observed for all fats around 10 °C. Increases in n around 10 °C indicated a change from one-dimensional to multi-dimensional growth. From the results of polarized light micrographs, the transformation from the coarser crystal structure to tiny crystal structure occurred in microstructure networks at the action of minor components.

1. Introduction

Palm kernel oil (PKO) and coconut oil (CNO) are rich in medium chain fatty acids (MCFA) and exhibit easy digestibility and absorbability. These outstanding properties make them useful for application in health food products. In addition, the high proportion of lauric acid in PKO and CNO gives their sharp melting properties, resulting in its application in fat-structured food materials, such as margarine, cocoa butter substitutes and ice cream (Pantzaris & Basiron, 2002).

PKO and CNO as fat-structured food materials could crystallize to form fat crystal network (Franke, Bindrich, & Heinz, 2015; Maleky, 2015; Ramel, Peyronel, & Marangoni, 2016), which impacts the mechanical and rheological properties of plastic fat. In many foods, the fat crystallization determines the consistency, plasticity sensory properties, physical stability, and appearance of fat-rich products (Marangoni et al., 2012). In addition, the presence of minor lipid components (diacylglycerols, monoacylglycerols and phospholipid) contributes significantly to the quality of various products (Maruyama et al., 2014). Therefore, it is imperative to study the influence of indigenous minor components on molecular structure, crystallization behavior, nano- and meso-scale structure of fat.

Fats and oils are mainly composed of triglycerides (> 95%) and small amounts of minor non-triglyceride components. The major minor components found in fats and oils include FFAs, MAGs, DAGs and PS (Smith, Bhaggan, Talbot, & van Malssen, 2011), which can influence the nucleation, the crystal growth, polymorphic transformation and microstructure (Patel & Dewettinck, 2015; Ribeiro et al., 2015; Smith et al., 2011). It has been reported that the crystallization kinetics was changed after removing minor compounds from milk fat (Wright, Hartel, Narine, & Marangoni, 2000) and that DAG increased the crystallization induction time of milk fat (Wright & Marangoni, 2002); while the overall kinetics of nucleation, crystal growth, and polymorphic transformation was delayed by the action of the minor components (Mazzanti, Guthrie, Sirota, Marangoni, & Idziak, 2004). In palm oil (PO), the high-melting monopalmitin (MP) initiated the crystallization process and induced a fractional crystallization of the PO triacylglycerols (TAG) (Verstringe, Danthine, Blecker, Depypere, & Dewettinck, 2013), and monoglycerides had the similar effect on the

* Corresponding author.
E-mail address: yfliu@jiangnan.edu.cn (Y. Liu).

https://doi.org/10.1016/j.foodres.2017.11.060
Received 29 June 2017; Received in revised form 20 November 2017; Accepted 22 November 2017
Available online 23 November 2017
0963-9969/

fully hydrogenated PO (Basso et al., 2010; Fredrick, Foubert, De Sype, & Dewettinck, 2008; Verstringe, Danthine, Blecker, & Dewettinck, 2014). Palm-based DAGs could also influence the nucleation and crystallization rate of PO (Saberi, Lai, & Toro-Vázquez, 2011). For CNO, dilauroylglycerol retarded nucleation while dioleoylglycerol had no significant effect (Gordon & Rahman, 1991). Also addition of lauric acid and low hydrophilic/lipophilic balance (low-HLB) sucrose esters also changed the isothermal crystallization kinetics of CNO (Chaleepa, Szepes, & Ulrich, 2010). Moreover, formation of smaller spherulites occurred for CNO after the emulsifier addition.

Despite the plethora of studies dealing with the influence of extraneous additives on crystallization, only few have focused on the impact of naturally existing minor components on fat crystal network. Therefore, the primary objective of this study was to investigate the influence of non-triglyceride components on the lipid composition, thermal properties, polymorphism, crystallization behavior, nanostructure and microstructure of PKO and CNO. In addition, the relationship between microstructure and crystallization kinetics were established for further analysis of the influence mechanism at the action of minor components.

2. Materials and methods

2.1. Materials

Palm kernel oil (PKO) (iodine value (IV) 17.61 g I_2/100 g and slip melting point (SMP) 27.12 °C) and coconut oil (CNO) (IV, 8.23 g I_2/100 g and SMP, 24.30 °C) were produced and donated generously by Kerry Specialty Fats Ltd. (Shanghai, China). Supelco 37 Component FAME mixture was purchased from Sigma-Aldrich China (Shanghai, China). All other chemicals and organic solvents of analytical or chromatographic grade purchased from Sinopharm Chemical Reagent Co. Ltd. (Shanghai, China) and Fisher Scientific (Shanghai, China), respectively.

2.2. Analysis of triglycerides, diglycedides, monoglycerides and free fatty acid in PKO and CNO

The contents of triglycerides, diglycedides, monoglycerides and free fatty acid in PKO and CNO were determined using Normal Phase HPLC (NPHPLC, refractive index detector) using a phenomenex Luna column (250 mm × 4.6 mm, 5 μm particle size) according to the previous method (Zeng, Qi, Xin, Yang, & Wang, 2015). The mobile phase was n-hexane and 2-propanol (15:1, v/v). The flow rate was 1 mL/min. Peaks in HPLC were evaluated by comparison of their retention times with those of known standards.

2.3. Separation of triacylglycerols from PKO and CNO

Purification of PKO and CNO was achieved using column chromatographic method (Siew & Ng, 1999). Briefly, a chromatographic glass column (2.5 cm diameter, 40 cm length) equipped with a Teflon stopcock was packed with 30 g of silica gel. 30 g of oil dissolved in 120 mL of petroleum ether were loaded onto the column and eluted with solvents into two fractions: the TAG of samples and the minor non-triglyceride components. The PKO-TAG and CNO-TAG were eluted with 95:5 petroleum ether/ethyl ether and subsequently more polar lipid components were eluted with diethyl ether. The progress of separation was monitored by thin-layer chromatography (TLC), which was performed on silica gel GF 254 plates (Haiyang Co. Ltd., Qingdao, China) with a developing solvent of hexane/diethyl ether/acetic acid (80/20/1, v/v/v). The bands were visualized using iodine vapor. The same fractions collected from multiple runs were combined, and the solvent was evaporated under vacuum.

2.4. Sliding melting point (SMP)

The SMP was determined by use of the AOCS standards method Cc3-25 (AOCS, American Oil Chemists' Society, 2009).

2.5. Fatty acid (FA) composition

FA composition was analyzed using a gas chromatography (GC) system (GC-2010PLUS, Shimadzu, Tokyo, Japan) equipped with a flame ionization detector (FID) and a fused-silica capillary column (TR-FAME, 60 m × 0.25 mm × 0.25 μm) according to AOCS Official Method Ce 2-66 (AOCS, 2009). The temperatures of the injector and FID detector were set at 50 and 250 °C, respectively. The column was heated to 60 °C and held for 3 min, then programmed at 5 °C/min to 175 °C, held for 15 min, then increased to 220 °C at 2 °C/min, and held for 10 min. The FA acids were identified by comparing their retention time to those of the FAME standards.

2.6. TAG composition

TAG composition of different samples was measured according to AOCS Official Method Ce 5-86 (AOCS, 2009) using an Agilent 7820A Series GC system (Agilent, California, USA) equipped with FID detector and a high temperature capillary column (Rtx-65TG, 30 m × 250 μm × 0.1 μm). The column temperature was initially held at 250 °C for 1 min, and then increased to 280 °C at a rate of 20 °C/min. The column temperature was then increased to 340 °C at a rate of 10 °C/min, and finally increased to 350 °C at a rate of 1 °C/min and held at 350 °C for 20 min. The carrier gas was hydrogen, and the total gas flow rate was 40 mL/min. The temperatures of the FID and injector were 360 and 350 °C, respectively. TAG profiles were determined according to the retention times of TAG standards.

2.7. Thermal analysis

The thermal properties of different samples were performed using a differential scanning calorimeter (DSC 8500, Perkin Elmer, USA) equipped with a liquid nitrogen cooling system according to literature method (Meng et al., 2010). Samples (5–10 mg) were hermetically sealed in an aluminum pan with an empty pan serving as reference. Samples were heated to 80 °C for 10 min to ensure complete melting and erasure of all crystal memory, and the crystallization profiles were obtained by cooling to − 40 °C at 5 °C/min. After a 10 min hold at this temperature, the melting profile was obtained by heating to 80 °C at 5 °C/min. All DSC analyses were performed in triplicate.

2.8. Solid fat content (SFC)

SFC was measured by pulsed nuclear magnetic resonance (*p*NMR) with a Bruker PC120 series NMR analyzer (Bruker, Karlsruhe, Germany). Water bath was used for rapid cooling and offered accurate temperature control. The instrument was automatically calibrated by use of three standards (supplied by Bruker) with the solid content of 0, 31.3, and 74.6%. Approximately 2.5 g of samples was placed in each glass NMR tube for all *p*NMR experiments and was kept at 80 °C for 30 min to ensure complete melting and destroy any crystal memory, and then placed in a thermostated water bath set at 0, 5, 10, 15, 20, 25, 30, 35 and 40 °C. All measurements were performed in triplicate.

For crystallization kinetics, *p*NMR was used to monitor changes in SFC as a function of time at different crystallization temperatures (5, 10, 15, 20, 25, 30 and 35 °C) according to literature method (Wright, Hartel, Narine, & Marangoni, 2000). Samples were heated at 80 °C for 30 min before analysis to destroy any crystal history. Three replicates of each preheated sample in glass NMR tubes were determined at each crystallization temperature and the SFC readings as a function of isothermal crystallization time were recorded by the equipment software

at least 10 min after achieving a sustained plateau in the measurements. Induction times of crystallization (τ_{SFC}) were also determined by extrapolating back to the onset time of the linear SFC increase based on the curves of SFC as a function of time. The data obtained under isothermal conditions were fitted to the Avrami equation by nonlinear regression. That is,

$$\frac{SFC(t)}{SFC(\infty)} = 1 - e^{-Kt^n}$$

Where, SFC(t) describes the SFC at crystallization time t, SFC(∞) is the limiting SFC as time approaches infinity, K is the crystallization rate constant and n is the Avrami exponent which is sensitive to the mechanism of crystallization.

These parameters take both the nucleation and crystal growth rates into account (Singh, Bertoli, Rousset, & Marangoni, 2004), which are influenced by both nucleation time and the dimensionality of growth. Half times of crystallization ($t_{1/2}$), reflect the magnitudes of the rate constants according to the following relationship:

$$t_{1/2} = \sqrt[n]{\frac{0.693}{K}}$$

2.9. Crystal polymorphism and crystalline domain size

X-ray diffraction (XRD) data were collected by use of D2 Phaser XRD (Bruker, Karlsrube, Germany) equipped with Cu-Kα radiation and Ni filter. The copper lamp (λ = 1.54 Å for copper) was set to 30 kV and 10 mA with the divergence slit, scatter slit, and receiving slit of 1.0,1.0 and 0.3 mm, respectively. For the small-angle X-ray diffraction analysis (SAXD) the samples were scanned from 1 to 10°. with 0.02°/min. The wide-angle X-ray diffraction analysis (WAXD) was obtained through scanning the samples from 11 to 30°. at 1°/min. Peak Fit software (Seasolve, Framingham, MA, USA) was used to analyze the obtained data in both SAXD and WAXD patterns. The analyses were performed at ambient temperature.

2.10. Crystal morphology

The morphology of crystallized samples were observed using polarized light microscopy (PLM) (DM2700P, Leica, Germany) with a Leica DFC450 video camera attached (Leica, Germany). The samples were held at 80 °C for 30 min to erase crystal memory. A small droplet (about 10 μL) of melted sample was placed on a preheated glass slide, using a preheated capillary tube and covered with a preheated coverslip, avoiding the introduction of air bubbles into the sample. Then the samples slides were transferred to temperature-controlled incubators (Linkam Instruments, Tadworth, U.K.) set at 5, 20 and 30 °C and observed under the microscope for up to 72 h.

The acquired images were then inverted, thresholded, and processed using with Adobe Photoshop (Adobe System Incorporated) according to the method described by Meng (Meng, Liu, Jin, Huang, Song, Wang, et al., 2010).

2.11. Statistical analysis

All experiments data were determined in triplicate and are reported as the means ± standard deviations (SD). The significance of the differences was analyzed by use of ANOVA with Duncan's multiple-range test using SPSS software. The significance of differences among mean values was identified at a level of $p < 0.05$.

3. Results and discussion

3.1. Contents of triglycerides and major non-triglyceride components in PKO and CNO

The principle minor non-triglyceride components in oils and fats are free fatty acids (FFA), monoacylglycerols(MAG), diacylglycerols (DAG) (Smith, Bhaggan, Talbot, & van Malssen, 2011). For PKO and CNO, the non-triglyceride components accounted for > 2 wt% of oil samples. PKO contained 97.9 wt% triglycerides (PKO-TAG) which is consistent well with previous reports (Relkin, Fabre, & Guichard, 2004; Smith, Cain, & Talbot, 2004). While, CNO accounted for 97.81 wt% triglycerides (CNO-TAG). For minor non-triglyceride polar lipids, diglycerides (DAGs), monoglycerides (MAG) and free fatty acids (FFAs) accounted for 1.48, 0.56 and 0.05 wt% in PKO and 1.61, 0.47 and 0.11 wt % in CNO (Dayrit, Buenafe, Chainani, & de Vera, 2008), respectively. Smith (Smith, Bhaggan, Talbot, & van Malssen, 2011) had pointed that minor components and additives with the addition of 0.5–5 wt% would be incorporated into fat crystals. In addition, the SMP decreased from 27.12 °C to 26.05 °C for PKO, and from 24.30 °C to 22.61 °C for CNO after removal of minor non-triglyceride components. So, removing of the minor non-triglyceride polar lipids in oil samples might change some aspects of crystallization leading to the difference of fat crystal network.

3.2. Lipid composition

As shown in Table 1, the fatty acid composition of the PKO and CNO was in agreement with the reports in the literature (Marina, Che Man, Nazimah, & Amin, 2009; Siew, 2001). The major fatty acids of PKO-TAG and PKO were the lauric acid ($C_{12:0}$, 48.53 and 50.51%, respectively), myristic acid ($C_{14:0}$, 16.11 and 15.82%, respectively) and oleic acid ($C_{18:1}$, 16.91 and 15.82%, respectively). In CNO-TAG and CNO, the predominant fatty acids were lauric acid ($C_{12:0}$, 49.19 and 49.13%, respectively), myristic acid ($C_{14:0}$, 18.50 and 18.26%, respectively), oleic acid ($C_{18:1}$, 7.29 and 7.22%, respectively). Compared to the PKO, CNO contained a significantly lower content of oleic acid $C_{18:1}$ ($p < 0.05$). However, no significantly differences appeared between the samples after removal of the minor components ($p > 0.05$) both in PKO and CNO. Therefore, the fatty acid composition remained unchanged after removing of minor non-triglyceride components whether in PKO or in CNO.

The TAG composition of PKO, PKO-TAG, CNO and CNO-TAG is presented in Table 1. The results of TAG composition obtained are also in accordance with coconut oil and pam kernel oil TAG ranges published in the literature (Chen, Chong, Ghazali, & Lai, 2007; Marina, Che Man, Nazimah, & Amin, 2009; Siew, 2001). The major TAG present in PKO and CNO samples consisted of LaLaLa, CCLa, CLaLa, LaLaM and LaMM. Compared the TAG composition of PKO with CNO, the contents of LaLaLa in PKO were more than those in CNO. However, there was no significant difference between the PKO and PKO-TAG, also the CNO and CNO-TAG. Therefore, removal of the minor non-triglyceride compositions did not affect the overall TAG composition of the bulk material.

3.3. Thermal behavior

Thermal profiles determined by differential scanning calorimeter (DSC) demonstrate transition of temperatures and heats in term of the melting and crystallization procedures of fats and oils. The melting and crystallization curves of PKO, PKO-TAG, CNO and CNO-TAG are presented in Fig. 1, respectively.

Upon cooling, two main exothermic peaks appeared in PKO, PKO-TAG, CNO and CNO-TAG, at the same cooling rate, representing low melting fraction and high melting fraction, respectively. Both of the two main exothermic peaks in PKO-TAG and CNO-TAG significantly shifted ($p < 0.05$) to lower temperatures in comparison to those of PKO and

Table 1
Lipid Composition (%) of PKO-TAG, PKO, CNO-TAG and CNO.

Lipid composition	CNO-TAG	CNO	PKO-TAG	PKO
Fatty acid				
$C_{6:0}$	0.28 ± 0.01	0.32 ± 0.00	0.10 ± 0.01	0.15 ± 0.02
$C_{8:0}$	5.68 ± 0.00	6.05 ± 0.07	1.77 ± 0.07	2.08 ± 0.35
$C_{10:0}$	4.36 ± 0.00	4.50 ± 0.04	2.17 ± 0.03	2.33 ± 0.11
$C_{12:0}$	49.19 ± 0.22	49.33 ± 0.05	48.53 ± 0.22	50.51 ± 0.61
$C_{14:0}$	18.50 ± 0.04	18.26 ± 0.03	16.11 ± 0.11	15.82 ± 0.19
$C_{16:0}$	9.37 ± 0.06	9.19 ± 0.01	8.85 ± 0.03	8.11 ± 0.30
$C_{18:0}$	2.77 ± 0.04	2.73 ± 0.01	2.20 ± 0.02	2.01 ± 0.06
$C_{18:1}$	7.29 ± 0.06	7.22 ± 0.15	16.91 ± 0.21	15.82 ± 0.04
$C_{18:2}$	1.69 ± 0.03	1.67 ± 0.01	2.48 ± 0.00	2.35 ± 0.10
Others[a]	0.87 ± 0.03	0.74 ± 0.02	0.81 ± 0.03	0.83 ± 0.01
Triglycerides[b]				
CaCaCa	1.28 ± 0.05	1.07 ± 0.16	3.34 ± 0.07	2.97 ± 0.09
CaCaLa	6.73 ± 0.04	6.11 ± 0.04	13.35 ± 0.03	12.59 ± 0.13
CaLaLa	9.11 ± 0.06	8.73 ± 0.06	17.26 ± 0.08	16.88 ± 0.07
LaLaLa	23.24 ± 0.14	23.14 ± 0.18	20.29 ± 0.11	20.46 ± 0.15
LaLaM	17.52 ± 0.06	17.40 ± 0.13	17.45 ± 0.13	17.77 ± 0.14
LaMM	10.44 ± 0.11	10.50 ± 0.09	10.81 ± 0.12	10.86 ± 0.16
LaLaS/LaPM	9.53 ± 0.03	9.79 ± 0.03	7.63 ± 0.02	7.93 ± 0.04
LaMS/LaPP	6.50 ± 0.01	7.00 ± 0.02	4.01 ± 0.08	4.24 ± 0.06
MPP	5.16 ± 0.03	5.53 ± 0.02	2.30 ± 0.07	2.54 ± 0.00
MOP	5.34 ± 0.02	5.54 ± 0.21	1.81 ± 0.01	1.81 ± 0.03
POP	2.45 ± 0.02	2.27 ± 0.06	1.20 ± 0.05	1.13 ± 0.01
POO	2.00 ± 0.01	1.91 ± 0.03	0.50 ± 0.06	0.81 ± 0.03
OOO	0.69 ± 0.00	1.02 ± 0.01	0.06 ± 0.00	0.02 ± 0.02

Values represent the average of three replicates ± standard deviation.
[a] "Others" refers to other fatty acids not identified by the FAME standards.
[b] TAG shown constitutes the major species present: Ca, capryloyl; D, caproyl; La, lauroyl; M, myristoyl; P, palmitoyl; S, stearoyl, O, oleoyl.

CNO. In addition, the exotherm (both two peaks) in cooling curves of PKO-TAG and CNO-TAG became smaller and sharper. These results could be attributed to the removal of minor components. The shift of peak to higher crystallization temperature at the presence of minor components was caused by that the minor components with surface-active properties could form the initial crystals in combination with high-melting TAGs (Cerdeira, Martini, Candal, & Herrera, 2006; Cerdeira, Martini, Hartel, & Herrera, 2003). Therefore, the minor non-triglyceride components increased the crystallization degree in the initial stages and also raised the temperature of nucleation from DSC crystallization profiles.

Except for temperature transition, the changes of enthalpy values reflected differences in the type, amount of crystals in fat crystal network (Li, Truong, & Bhandari, 2017). The released enthalpy variation (ΔH, J/g) of PKO-TAG and CNO-TAG in each big peak changed respectively after removal of the minor components as shown in Supplementary Table 1. Similar results were observed by the previous research (Ray, Smith, Bhaggan, Nagy, & Stapley, 2013). In comparison to PKO-TAG and CNO-TAG, higher released enthalpy variation of PKO and CNO indicated that the minor non-triglyceride components could improve the crystallization to form more perfect crystals (Ray et al., 2013).

The melting thermogram of PKO and CNO showed one big endothermic peak at 26.26 and 23.92 °C, respectively, and a small endothermic peak at 14.69 and 15.91 °C, respectively, with slightly moved toward lower temperature in PKO-TAG and CNO-TAG, as illustrated in Fig. 1A. According to Supplementary Table 1, the required enthalpy variations (ΔH, J/g) in each peak of PKO were 6.01 and 81.62 J/g and that of PKO-TAG was 101.28 J/g, with one small peak disappeared. For CNO, the required enthalpy variations (ΔH, J/g) in each peak were changed from 70.57 to 79.63 J/g for first peak, and from 106.86 to 107.67 J/g for second peak after removal of minor components. Therefore, the PKO and CNO crystallized and melted at higher temperature zone with an increased ΔH and at lower temperature zone with a decreased ΔH compared with the PKO-TAG and CNO-TAG ($p < 0.05$) suggesting that the existence of minor non-triglyceride polar components was contribute to the crystallization of PKO and CNO.

3.4. Crystal polymorphism and crystalline domain size

Crystal polymorphs of TAG could be determined based on the short spacings of crystals and the chain packing of fatty acid end group was characterized according to long spacings of crystals by use of X-ray diffraction (XRD). α, β', and β forms are the three basic polymorphic structures with the short spacing at 4.10 Å for α form, 4.2 and 3.8 Å for β' form, and 4.53 Å for β form. The long spacings of the fats represented the lamellar packing structure of nanoscale (Campbell, Goff, & Rousseau, 2002).

As shown in Fig.2, the polymorphic forms of the PKO, PKO-TAG, CNO and CNO-TAG were determined by XRD. In Fig. 2A, the short spacing patterns of 3.8 Å and 4.2 Å (for β' form) appeared in PKO, PKO-TAG, and the low-intensity peaks at 4.53 Å and 4.10 Å were discovered both in PKO and PKO-TAG, which characterized the polymorphic forms β and α form, respectively. In addition, a peak was observed with the short spacing of 4.53 Å for β form both in CNO and CNO-TAG. These results indicated that no polymorph transition occurred after removing of the minor non-triglyceride components. Therefore, the minor polar components did not changed the migration and agglomeration of TAGs in fats during the crystallization process, which agreed with a previous study (Wright, Hartel, Narine, & Marangoni, 2000).

In Fig. 2B, long spacing patterns of 33.4 (d_{001}) and 32.7 Å (d_{001}) were observed in PKO and PKO-TAG, respectively, which indicated a double chain length (2 L) stacking of TAGs. Both samples showed one long spacing peaks with a third-order (d_{003}) lamellar structure at 11.3 Å. Meanwhile, one relatively weaker signal with a second-order (d_{002}) lamellar structure both existed in the PKO and PKO-TAG at 16.9 Å. Additionally, CNO and CNO-TAG had the diffraction at the long spacing of 34.7 Å and 34.9 (d_{001}), respectively. The difference of one-order (d_{001}) lamellar structure indicated that the longitudinal packing form of TAGs in the PKO-TAG and CNO-TAG had changed to a certain degree in contrast to the PKO and CNO. In addition, the intensity and the shape of the diffraction peak was difference, which also indicated

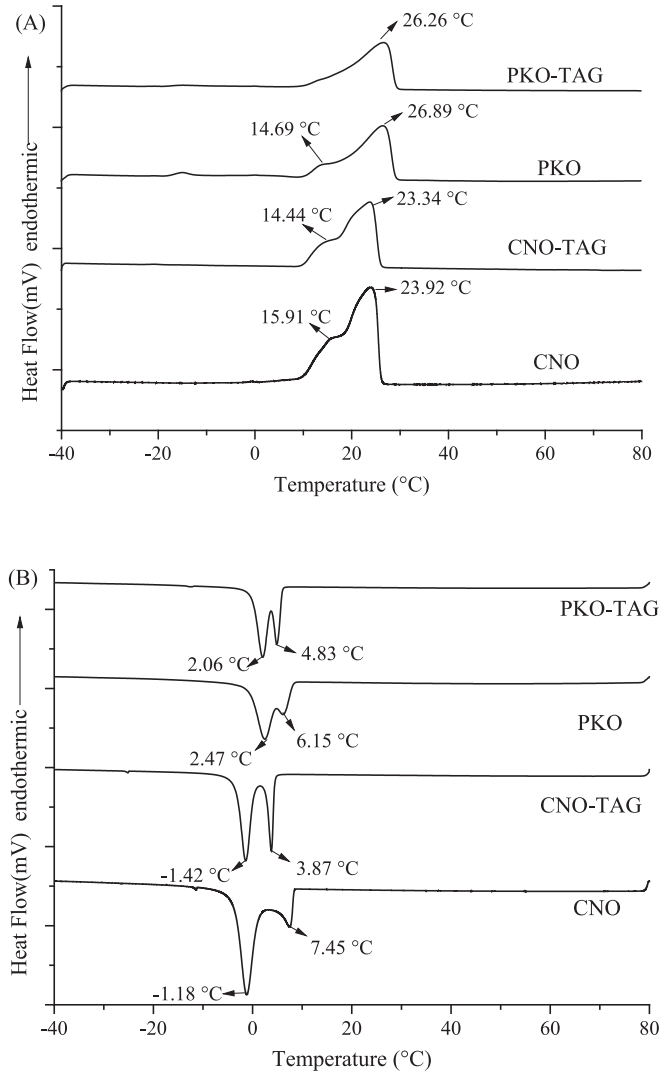

Fig. 1. DSC non isothermal crystallization curve and melting curves of PKO, PKO-TAG, CNO and CNO-TAG (A, melting curves; B, crystal1izaion curves).

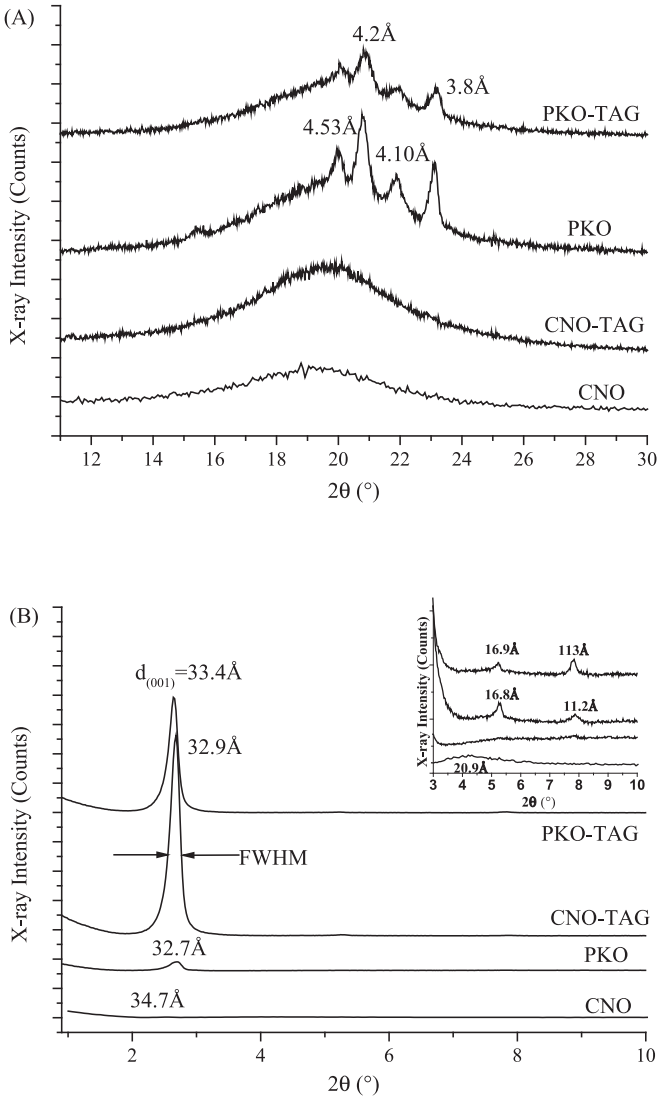

Fig. 2. WAXD (A) and SAXD (B) spectra for short and long spacings of PKO, PKO-TAG, CNO and CNO-TAG.

the change of the longitudinal packing state of TAGs. These could be due to the minor non-triglyceride components which were similar to the crystallization species could participate in the crystal matrix (Smith, Bhaggan, Talbot, & van Malssen, 2011).

In order to further analyze the difference of longitudinal packing state of TAGs, SAXD analysis was applied to evaluate the crystalline domain size (ξ) or the thickness of the nanoscale crystals by the well-known Scherrer formula (Acevedo & Marangoni, 2010).

$$\xi = \frac{k\lambda}{FWHMcos\theta}$$

Where k is the shape factor with a value of 0.9 for crystallites of unknown shape, θ is the diffraction angle, FWHM is the full width at half of the maximum of the Guassian fitting peak height in radians corresponding to the first small angle reflection reflecting the (001) plane, and λ is the XRD wavelength with the value of 1.54 Å for copper.

According to Scherrer formula and based on the FWHM in Fig. 2B (d_{001}), the crystalline domain size (thickness of a nanoscale-crystal) could be calculated. The crystalline domain size (i.e., thickness of a nanoscale-crystal) of PKO-TAG and PKO was 1595.71 ± 18.43 Å and 1285.65 ± 2.38 Å, respectively. The crystalline domain size of PKO-TAG was significantly bigger than that of PKO ($p < 0.05$). Similarly, the crystalline domain size (thickness of a nanoscale-crystal) of CNO-TAG was 1665.20 ± 2.35 Å, which was more than that (1395.67 ± 4.58 Å) of CNO significantly ($p < 0.05$). Therefore, the minor non-triglyceride components could take part in the crystallization of TAG molecules resulting in the change of lamellar packing structure of fats. This would further influence the change of microstructure of fats. In order to clarify this hypothesis, *p*NMR was used to measure crystallization kinetic and microstructure was determined by polarized light micrographs (PLM).

3.5. Solid fat content (SFC) and crystallization kinetics

The SFC decreased significantly as temperature increased ($p < 0.05$), but no differences were appeared after removing the minor non-triglyceride components (the Fig. was not shown), suggesting that the minor non-triglyceride components could not change the equilibrium SFC of fat.

To further study the influence of minor non-triglyceride components on the fat thermodynamics. The effects of minor components on crystallization kinetics were investigated by *p*NMR. As shown in Fig. 3, the SFC increased with the increase of crystallized time at different temperatures. Fig. 3A and B showed that both PKO and PKO-TAG crystallized very rapidly at high degree of supercooling with crystallization temperatures below 10 °C. There showed hyperbolic patterns against time and an equilibrium value in SFC was clearly visible in all curves.

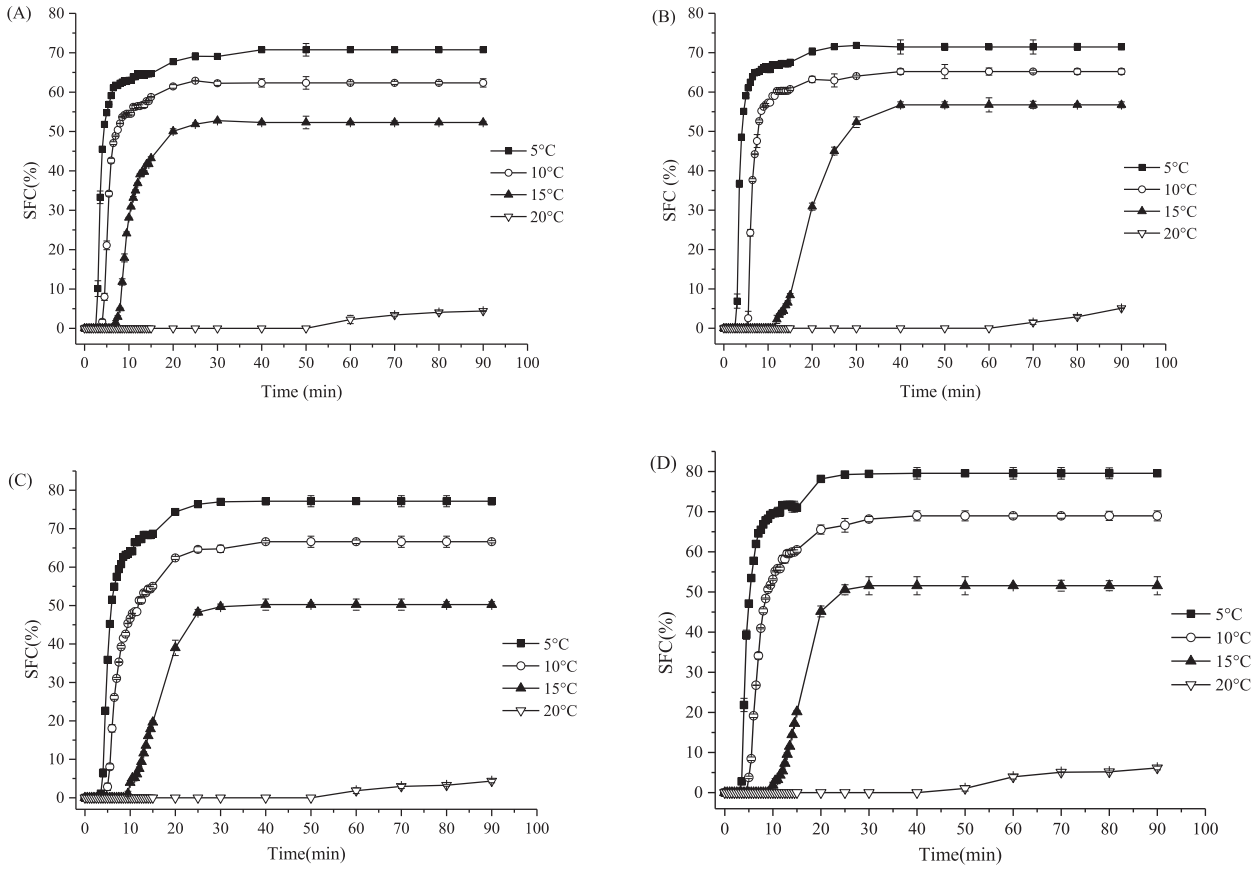

Fig. 3. Solid fat content versus time profile during isothermal crystallization of PKO (A), PKO-TAG (B), CNO (C) and CNO-TAG (D) at different crystallization temperatures. Symbols represent the average ± standard error of three replicates.

At low degree of supercooling (crystallization temperatures above 10 °C), there appeared no fat crystals during the initial lag period, followed by rapid crystallization to form sigmoidal curves. Similarly, two different regions were also occurred in CNO and CNO-TAG below and above 10 °C In addition, comparison of the curves of samples (PKO and CNO) and sample-TAGs (PKO-TAG and CNO-TAG) clearly showed that the latter had a steeper slop at each corresponding temperature, suggesting that the TAG had faster crystallization and shorter times to get maximum SFC.

In addition, induction times determined by SFC are shown in Table 2, the induction times of PKO were significantly lower than those of PKO-TAG ($p < 0.05$). Similar conclusion was also occurred between CNO and CNO-TAG. These results indicated that minor components had a promoting effect on induction times of crystallization. In addition, activation free energies of nucleation (ΔG) were related to induction times of crystallization (Herrera, de Leon Gatti, & Hartel, 1999). That is, shorter induction times translated into lower ΔG (Wright et al., 2000), which suggested that minor non-triglyceride components could decreased the energy barriers to nucleation.

Table 2
Induction time (min), Avrami Exponents (n), Avrami Constants (K), and half-times of crystallization ($t_{1/2}$) for PKO-TAG, PKO, CNO-TAG and CNO at different crystallization temperatures.

Temperature (°C)	τ_{SFC}[a](min)	n	K (min^{-n})	$t_{1/2}$ (min)	R^2
PKO					
5	2.48 ± 0.03[a]	1.016 ± 0.032[a]	0.293 ± 0.030[d]	2.338 ± 0.010[a]	0.992
10	3.76 ± 0.05[b]	1.142 ± 0.040[a]	0.161 ± 0.025[c]	3.597 ± 0.052[c]	0.987
15	6.71 ± 0.02[d]	3.815 ± 0.062[b]	0.008 ± 0.051[b]	9.104 ± 0.153[d]	0.964
PKO-TAG					
5	2.53 ± 0.03[a]	0.941 ± 0.065[a]	0.369 ± 0.091[e]	1.955 ± 0.134[b]	0.992
10	5.12 ± 0.02[c]	1.007 ± 0.081[a]	0.206 ± 0.063[d]	3.332 ± 0.124[c]	0.990
15	11.67 ± 0.06[e]	4.801 ± 0.173[b]	$3.593 \times 10^{-7} \pm 1.443 \times 10^{-8}$[a]	20.379 ± 0.819[e]	0.986
CNO					
5	3.03 ± 0.06[A]	1.085 ± 0.012[A]	0.161 ± 0.002[D]	3.8363 ± 0.034[A]	0.993
10	4.18 ± 0.08[B]	1.312 ± 0.014[A]	0.059 ± 0.013[C]	6.515 ± 0.024[C]	0.991
15	8.94 ± 0.12[D]	3.815 ± 0.057[B]	$1.598 \times 10^{-5} \pm 3.469 \times 10^{-6}$[B]	16.430 ± 0.532[E]	0.996
CNO-TAG					
5	3.15 ± 0.10[A]	0.848 ± 0.018[A]	0.303 ± 0.019[E]	2.655 ± 0.038[B]	0.999
10	4.66 ± 0.05[C]	1.298 ± 0.031[A]	0.073 ± 0.053[C]	5.692 ± 0.115[D]	0.987
15	9.27 ± 0.22[E]	5.288 ± 0.089[B]	$2.691 \times 10^{-7} \pm 6.543 \times 10^{-8}$[A]	32.431 ± 0.819[F]	0.996

Values represent the average of three replicates ± standard deviation. Different superscript letters (a–e) denote significantly difference ($p < 0.05$) for PKO and PKO-TAG, in the same column. Different superscript letters (A–E) denote significantly difference ($p < 0.05$) for CNO and CNO-TAG, in the same column. [b] "τ_{SFC}" refers to induction time by SFC.

3.6. Avrami analysis

The Avrami model is one of the useful methods to study the crystallization kinetics and evaluate the nature of crystal growth. As can be seen in Table 2, the SFC data fit the equation very well over the entire range of crystallization except at 20 °C ($R^2 > 0.96$ in all case).

The Avrami constants (K) decreased significantly with the increase of crystallization temperature at 5 and 10 °C, suggesting faster crystallization at a higher degree of supercooling. For PKO and PKO-TAG, the Avrami constant was strong influenced by crystallization temperature at 10 and 15 °C ($p < 0.001$). Here, the K value dropped by factors of roughly 10^2 (PKO) and 10^6 (PKO-TAG) in contrast to the values at 15 °C, respectively. For CNO and CNO-TAG, similar behavior was also appeared. Correspondingly, the Avrami constants changed significantly at the crystallization temperature of 10 °C. The change of K values was a combined affection by the nucleation and/or growth rate of crystallization at different temperature, which indicated the changes of the crystal type and size, spatial arrangement of crystals and intercrystalline interaction. As shown in Table 2, PKO had significantly lower Avrami constants than PKO-TAG ($p < 0.05$) at 10 and 15 °C, and similar regulation was occurred between the CNO and CNO-TAG, suggesting that the native mixture of minor non-triglyceride components could affect the crystallization rate of samples. In addition, the $t_{1/2}$ increased with the increase of crystallization temperature, which also indicated the K values decreased at higher temperature. By comparing the K and $t_{1/2}$ of PKO and PKO-TAG at each crystallization temperature, it was clear that the latter had higher K values and lower $t_{1/2}$ values ($p < 0.05$). For CNO and CNO-TAG, faster crystallization of CNO-TAG was also occurred with the increase of parameter K and the decrease in $t_{1/2}$ in contrast to the CNO at the same crystallization. These results indicated that the native mixture of minor non-triglyceride components could slow down the crystallization rate of PKO which was in agreement with previous isothermal crystallization curves (Fig. 3). This contributed to the adsorption of minor non-triglyceride components at the crystallization kink sites, and prevented the other TAG molecules from joining the crystals (Smith & Povey, 1997).

n reflects the number of fat crystal network dimensions during the fat crystallization process which indicated the mechanisms of nucleation and growth. As can be seen in Table 2, the Avrami exponent n for all samples increased with crystallization temperature increase. However, no significance difference appeared between the oil samples (PKO and CNO) and sample-TAGs (PKO-TAG and CNO-TAG) at 5 and 10 °C. These might be due to the minor non-triglyceride components could not affect the type of nucleation and growth with more rod-like growth at lower crystallization temperature. Whereas at a set temperature of 15 °C, the value of n was slightly lower in the samples with no minor non-triglyceride components (PKO-TAG and CNO-TAG), which indicated that remove of minor non-triglyceride components promoted the crystallization rate resulting in large crystal sizes.

3.7. Microscopy and fractal dimension

The microstructures of the fat samples were determined by PLM in order to evaluate the effects of minor non-triglyceride components on fat crystal network structure. Micrographs obtained after crystallization at 5 and 15 °C for 24 h are shown in Fig. 4, respectively.

Some significant differences were occurred among the different fat samples including the crystal number and crystallite diameter. The PKO showed smaller and more numerous spherical crystals relative to the PKO-TAG. For example, under the condition of 5 °C, compared with PKO-TAG, the crystals of PKO had great differences in morphology. Because of existing of minor components, the crystalline particles of PKO tended to be more delicate, fine and uniform particles. However, the crystals of PKO-TAG were aggregation to be relatively larger after purification of PKO, resulting in a different fat crystal network. These results indicated that minor non-triglyceride components could participate in the aggregation of the molecular leading the change of the fat crystal network so as to affect the formation of crystal microstructure. Similar trends occurred between the CNO and CNO-TAG further validated the influence of the minor non-triglyceride components on the fat crystal network. As shown in Fig.4, CNO also had a different crystalline morphology compared with CNO-TAG. The CNO showed smaller and more numerous crystals in contrast to the CNO-TAG, especially at 5 °C. These differences in microstructure correspond to the regulation observed in Avrami analysis.

In addition, it is obvious that the influence of temperature on crystal network structure. For PKO and CNO, two different networks appeared at different temperature, that is, there displayed a bigger and less numerous crystal with the temperature increased and so as PKO-TAG and CNO-TAG. With a high degree of supercoiling at 5 °C, nucleation proceeded very rapidly and resulted in pattern of crystal structure resembles a starry night. However, at higher temperature (15 °C), there was more time for the crystals to arrange into more ordered microstructure, the molecule aggregated and then continued to grow larger, resulting in the formation of medium or larger sized clusters, which further aggregate to different fat crystal network.

The fractal dimension (D_f) obtained by the particle counting method can be used to evaluate the spatial distribution of the crystals in the crystal network. There were no difference about the fractal dimensions between the PKO and PKO-TAG at the crystallization temperature of 5 °C (Fig. 4). However, the fractal dimensions (D_f) of PKO-TAG were significantly lower than that of PKO at 15 °C. Similar trends occurred between the CNO and CNO-TAG. These results suggested that minor non-triglyceride components could participate in the crystallization and promote the nucleation and growth process to be more ordered resulting in higher fractal dimensions in network at low supercooling conditions (15 °C). In addition, as the crystallization temperature increase, the fractal dimensions decreased significantly ($p < 0.05$) which was in accordance with the research of Marangoni (Alejandro Marangoni & McGauley, 2003). Moreover, the photomicrograph showed larger crystals aggregated to form larger clusters (Fig.4). These larger clusters could entrap more liquid oils leading to less cluster-cluster interactions and resulting in a weaker crystal network and less ordered structured at high temperature. These also suggested that minor non-triglyceride components strengthen the cluster-cluster interactions of the crystal networks.

4. Conclusions

In the present study, the presence of minor non-triglyceride components could significantly affect the fat crystal network of PKO and CNO. The minor non-triglyceride components with surface-active properties could form the initial crystals in the initial stages of crystallization, in combination with high-melting TAGs, resulting in shorter induction times of crystallization and higher temperature of nucleation from DSC crystallization profiles. However, the crystal growth rate was considerably decreased because of the adsorption of minor non-triglyceride components at the crystallization kink sites, preventing the other TAG molecules from joining the crystal. In addition, the minor non-triglyceride components had no influence on transformation of morphology of crystals, but the thickness of the single crystallites decreased resulting in the change of fat crystal network. Consequently, the transformation from the coarser crystal structure to tiny crystal structure occurred in microstructure networks at the action of minor non-triglyceride components. Moreover, the minor non-triglyceride components could participate in the crystallization process of TAG, leading to the formation of perfect structure of fat for applications in food industry.

Brief descriptions in nonsentence format listing the contents of the files supplied as Supporting Information. Table of thermal property of PKO, PKO-TAG, CNO and CNO-TAG. Supplementary data associated with this article can be found in the online version, at https://doi.org/

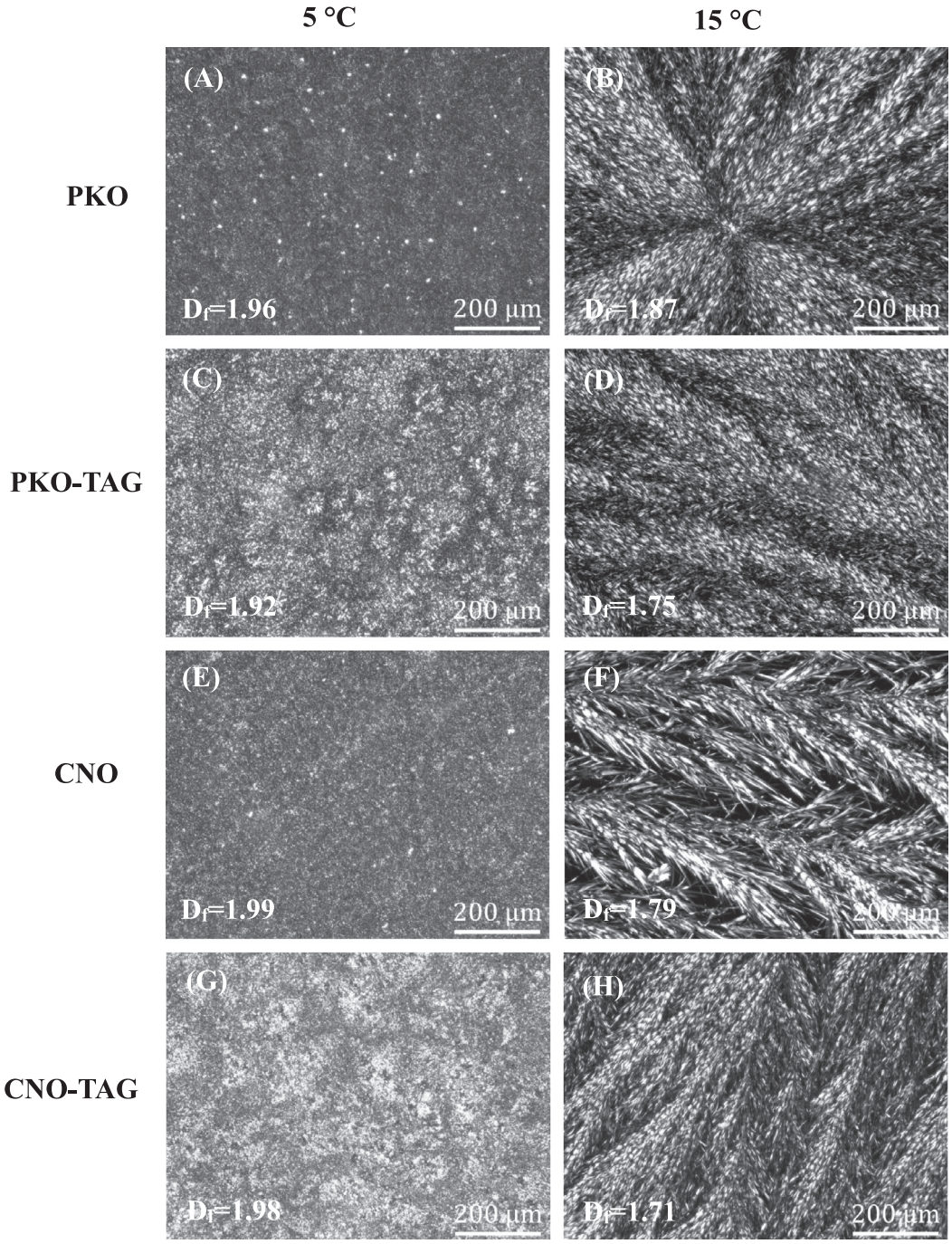

Fig. 4. Polarized light micrographs of samples crystallized for 24 h at different temperatures: (A) 5 °C for PKO, (B) 15 °C for PKO, (C) 5 °C for PKO-TAG, (D) 15 °C for PKO-TAG, (E) 5 °C for CNO, (F) 15 °C for CNO, (G) 5 °C for CNO-TAG, (H) 15 °C for CNO-TAG.

10.1016/j.foodres.2017.11.060.

Conflict of interest

The authors declare no conflict of interest

Abbreviations

PKO	palm kernel oil
CNO-TAG	triglycerides of palm kernel oil
CNO	coconut oil
CNO-TAG	triglycerides of coconut oil
PO	palm oil
FFA	free fatty acid
DAG	diacylglycerol
MAG	monoacylglycerols
MP	monopalmitin
TAG	triacylglycerol
DSC	differential scanning calorimetry
XRD	X-ray diffraction
IV	iodine value
SMP	slip melting point
PLM	polarized light microscopy
TLC	thin-layer chromatography
ANOVA	analysis of variance

Acknowledgement

This research was funded by Rich Products Corporation (USA). This research was supported by the National Key Research and Development Program of China (2016YFD0401404), and the National Natural Science Foundation of China (31772008, 31471678).

References

Acevedo, N. C., & Marangoni, A. G. (2010). Characterization of the nanoscale in triacylglycerol crystal networks. *Crystal Growth and Design, 10*(8), 3327–3333.

AOCS, American Oil Chemists' Society (2009). *Official methods and recommended practices of the American Oil Chemists' Society (6th ed.), Champaign*.

Basso, R. C., Ribeiro, A. P. B., Masuchi, M. H., Gioielli, L. A., Gonçalves, L. A. G., Santos, A. O.d., ... Grimaldi, R. (2010). Tripalmitin and monoacylglycerols as modifiers in the crystallisation of palm oil. *Food Chem, 122*(4), 1185–1192.

Campbell, S. D., Goff, H. D., & Rousseau, D. (2002). Comparison of crystallization properties of a palm stearin/canola oil blend and lard in bulk and emulsified form. *Food Res Int, 35*(10), 935–944.

Cerdeira, M., Martini, S., Candal, R. J., & Herrera, M. L. (2006). Polymorphism and growth behavior of low-trans fat blends formulated with and without emulsifiers. *J Am Oil Chem Soc, 83*(6), 489–496.

Cerdeira, M., Martini, S., Hartel, R. W., & Herrera, M. L. (2003). Effect of sucrose ester addition on nucleation and growth behavior of milk fat − sunflower oil blends. *J Agric Food Chem, 51*(22), 6550–6557.

Chaleepa, K., Szepes, A., & Ulrich, J. (2010). Effect of additives on isothermal crystallization kinetics and physical characteristics of coconut oil. *Chem Phys Lipids, 163*(4), 390–396.

Chen, C. W., Chong, C. L., Ghazali, H. M., & Lai, O. M. (2007). Interpretation of triacylglycerol profiles of palm oil, palm kernel oil and their binary blends. *Food Chem, 100*(1), 178–191.

Dayrit, F. M., Buenafe, O. E., Chainani, E. T., & de Vera, I. M. (2008). Analysis of monoglycerides, diglycerides, sterols, and free fatty acids in coconut (*Cocos nucifera* L.) oil by ^{31}P NMR spectroscopy. *Journal of Agricultural & Food Chemistry, 56*(56), 5765–5769.

Franke, K., Bindrich, U., & Heinz, V. (2015). Fat crystal network structures have a strong influence on properties of fat-based barrier layers. *Eur J Lipid Sci Technol, 117*(11), 1792–1800.

Fredrick, E., Foubert, I., De Sype, J. V., & Dewettinck, K. (2008). Influence of monoglycerides on the crystallization behavior of palm oil. *Crystal Growth and Design, 8*(6), 1833–1839.

Gordon, M. H., & Rahman, I. A. (1991). Effects of minor components on the crystallization of coconut oil. *J Am Oil Chem Soc, 68*(8), 577–579.

Herrera, M., de Leon Gatti, M., & Hartel, R. (1999). A kinetic analysis of crystallization of a milk fat model system. *Food Res Int, 32*(4), 289–298.

Li, B.-Z., Truong, T., & Bhandari, B. (2017). Crystallization and melting properties of mixtures of milk fat stearin and omega-3 rich oils. *Food Chem, 218*, 199–206.

Maleky, F. (2015). Nanostructuring triacylglycerol crystalline networks under external shear fields: A review. *Curr Opin Food Sci, 4*, 56–63.

Marangoni, A. G., Acevedo, N., Maleky, F., Co, E., Peyronel, F., Mazzanti, G., ... Pink, D. (2012). Structure and functionality of edible fats. *Soft Matter, 8*(5), 1275–1300.

Marangoni, A. G., & McGauley, S. E. (2003). Relationship between crystallization behavior and structure in cocoa butter. *Crystal Growth and Design, 3*(1), 95–108.

Marina, A. M., Che Man, Y. B., Nazimah, S. A. H., & Amin, I. (2009). Chemical properties of virgin coconut oil. *J Am Oil Chem Soc, 86*(4), 301–307.

Maruyama, J. M., Soares, F. A. S. D. M., D'Agostinho, N. R., Gonçalves, M. I.s. A., Gioielli, L. A., & da Silva, R. C. (2014). Effects of emulsifier addition on the crystallization and melting behavior of palm olein and coconut oil. *J Agric Food Chem, 62*(10), 2253–2263.

Mazzanti, G., Guthrie, S. E., Sirota, E. B., Marangoni, A. G., & Idziak, S. H. (2004). Effect of minor components and temperature profiles on polymorphism in milk fat. *Crystal Growth and Design, 4*(6), 1303–1309.

Meng, Z., Liu, Y. F., Jin, Q. Z., Huang, J. H., Song, Z. H., Wang, F. Y., & Wang, X. G. (2010). Characterization of graininess formed in all beef tallow-based shortening. *J Agric Food Chem, 58*(21), 11463–11470.

Pantzaris, T. P., & Basiron, Y. (2002). The lauric (coconut and palm kernel) oils. In F. D. Gunstone (Ed.). *Vegetable oils in food technology: Composition, properties and uses* (pp. 157–201). Blackwell Publishing: CRC Press, USA.

Patel, A. R., & Dewettinck, K. (2015). Current update on the influence of minor lipid components, shear and presence of interfaces on fat crystallization. *Curr Opin Food Sci, 3*, 65–70.

Ramel, P. R. R., Jr., Peyronel, F., & Marangoni, A. G. (2016). Characterization of the nanoscale structure of milk fat. *Food Chem, 203*, 224–230.

Ray, J., Smith, K. W., Bhaggan, K., Nagy, Z. K., & Stapley, A. G. (2013). Crystallization and polymorphic behavior of shea stearin and the effect of removal of polar components. *Eur J Lipid Sci Technol, 115*(10), 1094–1106.

Relkin, P., Fabre, M., & Guichard, E. (2004). Effect of fat nature and aroma compound hydrophobicity on flavor release from complex food emulsions. *J Agric Food Chem, 52*(20), 6257–6263.

Ribeiro, A. P. B., Masuchi, M. H., Miyasaki, E. K., Domingues, M. A. F., Stroppa, V. L. Z., de Oliveira, G. M., & Kieckbusch, T. G. (2015). Crystallization modifiers in lipid systems. *J Food Sci Technol, 52*(7), 3925–3946.

Saberi, A. H., Lai, O.-M., & Toro-Vázquez, J. F. (2011). Crystallization kinetics of palm oil in blends with palm-based diacylglycerol. *Food Res Int, 44*(1), 425–435.

Siew, W. L. (2001). Crystallisation and melting behaviour of palm kernel oil and related products by differential scanning calorimetry. *Eur J Lipid Sci Technol, 103*(11), 729–734.

Siew, W. L., & Ng, W. L. (1999). Influence of diglycerides on crystallisation of palm oil. *J Sci Food Agric, 79*(5), 722–726.

Singh, A. P., Bertoli, C., Rousset, P. R., & Marangoni, A. G. (2004). Matching avrami indices achieves similar hardnesses in palm oil-based fats. *J Agric Food Chem, 52*(6), 1551–1557.

Smith, K. W., Bhaggan, K., Talbot, G., & van Malssen, K. F. (2011). Crystallization of fats: Influence of minor components and additives. *J Am Oil Chem Soc, 88*(8), 1085–1101.

Smith, K. W., Cain, F. W., & Talbot, G. (2004). Nature and composition of fat bloom from palm kernel stearin and hydrogenated palm kernel stearin compound chocolates. *J Agric Food Chem, 52*(17), 5539–5544.

Smith, P. R., & Povey, M. J. (1997). The effect of partial glycerides on trilaurin crystallization. *J Am Oil Chem Soc, 74*(2), 169–171.

Verstringe, S., Danthine, S., Blecker, C., Depypere, F., & Dewettinck, K. (2013). Influence of monopalmitin on the isothermal crystallization mechanism of palm oil. *Food Res Int, 51*(1), 344–353.

Verstringe, S., Danthine, S., Blecker, C., & Dewettinck, K. (2014). Influence of a commercial monoacylglycerol on the crystallization mechanism of palm oil as compared to its pure constituents. *Food Res Int, 62*, 694–700.

Wright, A. J., Hartel, R. W., Narine, S. S., & Marangoni, A. G. (2000). The effect of minor components on milk fat crystallization. *J Am Oil Chem Soc, 77*(5), 463–475.

Wright, A. J., & Marangoni, A. G. (2002). Effect of DAG on milk fat TAG crystallization. *J Am Oil Chem Soc, 79*(4), 395–402.

Zeng, C.-X., Qi, S.-J., Xin, R.-P., Yang, B., & Wang, Y.-H. (2015). Enzymatic selective synthesis of 1, 3-DAG based on deep eutectic solvent acting as substrate and solvent. *Bioprocess Biosyst Eng, 38*(11), 2053–2061.